

# Beyond AlphaEarth: Toward Human-Centered Spatial Representation via POI-Guided Contrastive Learning

Junyuan Liu<sup>a</sup>, Quan Qin<sup>a,b</sup>, Guangsheng Dong<sup>a,c</sup>, Xinglei Wang<sup>a</sup>, Jiazhuang Feng<sup>a</sup>, Zichao Zeng<sup>a</sup>, Tao Cheng<sup>a,\*</sup>

<sup>a</sup>*SpaceTimeLab, Department of Civil, Environmental and Geomatic Engineering, University College London, London, WC1E 6BT, United Kingdom*

<sup>b</sup>*School of Resource and Environmental Sciences, Wuhan University, Wuhan, 430079, China*

<sup>c</sup>*State Key Laboratory of Information Engineering in Surveying, Mapping and Remote Sensing, Wuhan University, Wuhan, 430079, China*

---

## Abstract

General-purpose spatial representations are essential for building transferable geospatial foundation models (GFMs). Among them, the AlphaEarth Foundation (AE) represents a major step toward a global, unified representation of the Earth's surface, learning 10-meter embeddings from multi-source Earth Observation (EO) data that capture rich physical and environmental patterns across diverse landscapes. However, such EO-driven representations remain limited in capturing the functional and socioeconomic dimensions of cities, as they primarily encode physical and spectral patterns rather than human activities or spatial functions. We propose **AETHER** (AlphaEarth-POI Enriched Representation Learning), a lightweight framework that adapts AlphaEarth to human-centered urban analysis through multimodal alignment guided by Points of Interest (POIs). AETHER aligns AE embeddings with textual representations of POIs, enriching physically grounded EO features with semantic cues about urban functions and socioeconomic contexts. In Greater London, AETHER achieves consistent gains over the AE baseline, with a 7.2% relative improvement in land-use classification F1 and a 23.6% relative reduction in Kullback–Leibler divergence for socioeconomic mapping. Built upon pretrained AE, AETHER leverages a lightweight multimodal alignment to enrich it with human-centered semantics while remaining computationally efficient and scalable for urban applications. By coupling EO with human-centered semantics, it advances geospatial foundation models toward general-purpose urban representations that integrate both physical form and functional meaning.

**Keywords:** Geospatial Foundation Model, AlphaEarth, POI, Contrastive Learning, Urban Representation Learning

---

## 1. Introduction

Understanding the spatial organization and functional dynamics of cities remains a long-standing challenge in GIScience and urban computing. Addressing this challenge requires spatial representations that generalize across scales, modalities, and urban contexts. Recent advances in geospatial foundation models (GFMs) begin to meet this need by learning geographic embeddings from large-scale Earth Observation (EO) data (Klemmer et al., 2023; Yan et al., 2024). Among these, the AlphaEarth Foundation model (Brown et al., 2025) stands out as one of the most comprehensive efforts to date, producing 64-dimensional embeddings at 10-meter resolution from multi-source satellite imagery. For simplicity, we refer to it as AlphaEarth (AE) hereafter. These embeddings excel in natural land-surface tasks such as land-cover classification and ecological mapping, showcasing the potential of large-scale visual pretraining for spatial understanding.

However, transferring such representations to urban contexts remains challenging. Urban environments are shaped not only by their physical morphology but also by human activities, infrastructures, and socioeconomic interactions (Batty, 2013). While AE offers uniform, globally consistent coverage, its embeddings predominantly encode optical

---

\*Corresponding author.

Email address: [tao.cheng@ucl.ac.uk](mailto:tao.cheng@ucl.ac.uk) (Tao Cheng)

and environmental signals, limiting their ability to capture the functional organization of urban systems. Bridging this gap requires integrating information that reflects how people use, experience, and structure urban space.

Points of Interest (POIs) provide precisely such human-centered cues, carrying information about both the “where” (spatial) and the “what” (platial) aspects of urban environments (Goodchild, 2020). By linking locational attributes with semantic labels, POIs offer valuable insights into how people organize, perceive, and utilize urban space. A growing body of research has incorporated POI information into urban modeling to capture human activity patterns and functional structures (Yan et al., 2017; Niu and Silva, 2021; Huang et al., 2022). However, most existing studies still lack a comprehensive understanding of the rich semantic context embedded in POI data. Recent efforts, such as the CaLLiPer framework (Wang et al., 2025; Liu et al., 2025), have sought to address this limitation by explicitly integrating locational and semantic embeddings to learn more expressive representations of urban functions. Despite these advances, the spatial distribution of POIs remains highly uneven. They are dense in commercial cores but sparse in peripheral or residential areas and biased toward specific economic or institutional categories. Consequently, POI-derived representations alone lack completeness and spatial balance.

These challenges motivate a key research question: How can we combine the evenly distributed, physically grounded embeddings of AE with the discrete but functionally rich signals of POIs to obtain holistic urban representations? Our central idea is that by aligning AE and POI embeddings in a shared latent space, a model can learn latent correspondences between urban morphology and human function, allowing physical patterns to be enriched with socioeconomic semantics.

To this end, we propose **AETHER** (AlphaEarth–POI Enriched Representation Learning), a multimodal alignment framework that adapts AE for human-centered urban analysis. AETHER aggregates AE’s embeddings within spatial buffers around POI locations, projects them through designed multi-scale heads, and aligns them with POI text embeddings derived from pretrained language models using an InfoNCE-based contrastive objective. The aligned embeddings can then be aggregated into region-level features for downstream applications.

We consider two representative downstream tasks to evaluate AETHER’s effectiveness: land-use classification (LUC) and socioeconomic distribution mapping (SDM). These tasks are complementary in their reliance on distinct aspects of urban representation. LUC primarily depends on physical and morphological characteristics, such as built-up density, vegetation cover, and spatial texture. In contrast, SDM focuses on predicting human-centered and socioeconomic attributes that are not directly reflected in physical form but are strongly correlated with functional semantics.

We conduct experiments in Greater London, where AETHER consistently outperforms both AE-only and POI-only baselines across LUC and SDM tasks. Results demonstrate that multimodal alignment substantially enhances the functional interpretability of EO-based representations while maintaining computational efficiency and robustness across hyperparameters and supervision scales. By enriching physical embeddings with human-centered information, AETHER establishes a scalable foundation for bridging environmental and socioeconomic perspectives in urban modeling.

In summary, the main contributions of this study are:

- **First extension of AlphaEarth toward human-centered understanding.** To the best of our knowledge, AETHER is the first to extend AE beyond its original EO objectives by integrating human-centric semantic information through POI-guided alignment, enabling representations that capture both physical and functional dimensions of urban environments.
- **A POI-guided, multi-scale multimodal alignment framework.** We design an efficient contrastive-learning mechanism that connects AE embeddings with POI representations across multiple spatial scales, capturing cross-modal correspondences between physical form and functional roles.
- **Comprehensive empirical validation.** Through experiments in Greater London, AETHER achieves state-of-the-art performance on both land-use and socioeconomic mapping tasks, demonstrating strong robustness and data efficiency across diverse urban settings.

For reproducibility and further research, our implementation is publicly available at <https://github.com/inwind0212/AETHER>.

## 2. Related Work

### 2.1. Spatial Representations from Diverse Data

Spatial representation learning has drawn on a diverse range of geospatial data sources, each emphasizing different aspects of the Earth’s surface and human environment. Depending on their origin and information content, these data give rise to distinct modeling paradigms that capture spatial configuration, physical morphology, semantic functions, and dynamic activities from different perspectives. Accordingly, existing studies can be broadly grouped into four major lines: location-based, imagery-based, and POI-based representations.

Location encoding transforms geographic coordinates into continuous embeddings usable by neural networks (Mai et al., 2022). Typical methods learn a mapping  $y = \text{NN}(\text{PE}(\lambda, \phi))$ , where positional encodings (PE) of coordinates  $(\lambda, \phi)$  are passed through a neural network. Approaches such as Wrap (Mac Aodha et al., 2019), Space2Vec (Mai et al., 2020), Sphere2Vec (Mai et al., 2023), and Spherical Harmonics (Rußwurm et al., 2024) generate smooth, inductive spatial representations that capture geographic continuity and spatial autocorrelation. While these models provide dense spatial coverage and strong generalization, they primarily encode *where* places are rather than *what* they mean or *how* they function—leaving semantic understanding to be addressed by multimodal alignment frameworks.

Remote sensing and street-level imagery have long served as fundamental data sources for space understanding. In geospatial research, large-scale pretraining frameworks, such as SatCLIP (Klemmer et al., 2023) and GeoCLIP (Vivanco Cepeda et al., 2024), align satellite imagery with geographic coordinates to generate general-purpose embeddings. AlphaEarth (Brown et al., 2025) further integrates multi-source EO data into 10 m embeddings that capture detailed land-surface morphology and environmental context. However, these EO-driven models primarily encode physical and spectral features, limiting their ability to represent human functions or socioeconomic structures.

POIs provide a complementary and human-centered view of cities. Each POI conveys semantic information through its location, category, and name about the role of a place, such as education, commerce, or healthcare. Early models like Place2Vec (Yan et al., 2017), Doc2Vec Niu and Silva (2021) and Location2Vec (Qin et al., 2022) leveraged spatial co-occurrence among POIs, while graph-based methods (Xu et al., 2022; Su et al., 2023; Huang et al., 2023, 2022; Qin et al., 2025) modeled functional connectivity among locations. These representations highlight the richness of POI data but still offer limited semantic abstraction. The recent CaLLiPer framework (Wang et al., 2025; Liu et al., 2025) advances this line of work by aligning POI text embeddings generated by advanced language models, enabling a deeper understanding of urban functions and semantics.

Taken together, each data modality offers a unique but incomplete perspective on urban space: coordinate data emphasize spatial configuration, imagery captures physical morphology, and POIs encode functional semantics. Integrating these complementary signals motivates recent efforts toward multimodal urban representation learning, where contrastive alignment has emerged as a powerful mechanism for unifying heterogeneous sources.

### 2.2. Multimodal Alignment and Contrastive Learning

To overcome the limitations of single-modality representations, recent research increasingly focuses on multimodal alignment frameworks that bridge heterogeneous geospatial signals. Inspired by CLIP (Radford et al., 2021), contrastive learning has become a key paradigm for aligning diverse modalities within a shared embedding space, effectively integrating spatial, visual, and semantic information. In geospatial domains, this idea has been applied to image–location (Klemmer et al., 2023; Vivanco Cepeda et al., 2024), image–text (Yan et al., 2024; Bai et al., 2023), and POI–location pairings (Wang et al., 2025; Liu et al., 2025), demonstrating its potential to unify physical and functional perspectives of space.

Recent multimodal works have expanded this paradigm in different directions. UrbanCLIP (Yan et al., 2024) employed language-generated captions for satellite imagery to inject textual semantics into visual encoders; Bai et al. (Bai et al., 2023) jointly embedded very-high-resolution (VHR) imagery and POIs for unsupervised functional mapping; MobCLIP (Wen et al., 2025) further generalized contrastive alignment by coupling human mobility data with multimodal urban signals, achieving strong cross-domain transfer; and CaLLiPer (Wang et al., 2025; Liu et al., 2025) provided a lightweight POI–location alignment framework that integrates spatial and textual semantics for urban function prediction. Together, these studies illustrate the effectiveness of contrastive objectives and projection-based alignment in capturing urban semantics beyond visual appearance.

Nevertheless, most existing multimodal frameworks still rely on shallow pairwise alignments and have not exploited the dense spatial continuity or global consistency of Earth-Observation foundation models. Few efforts have

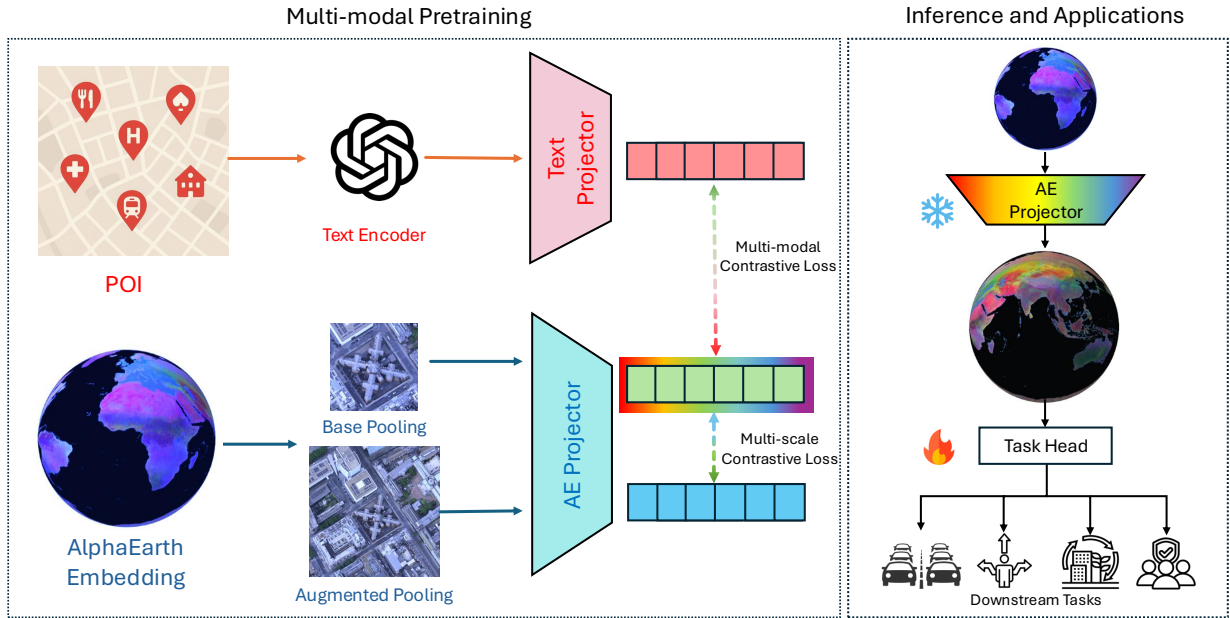


Figure 1: Overview of the proposed AETHER framework. During multimodal pretraining (left), AE embeddings within dual spatial buffers (base 50 m, augmented 100 m) are pooled and projected, while POI text embeddings are generated via a text encoder and projector. Two contrastive losses are applied: a cross-modal AE-POI alignment loss and an intra-modal multi-scale AE consistency loss (weighted by  $\lambda$ ). During inference (right), only the frozen AE projector is used to generate city-wide embeddings, which are aggregated to region-level features and passed into task heads for downstream applications.

explored aligning physically grounded EO embeddings from AE with human-centered semantics. This motivates our work: AETHER adapts AE to urban contexts through POI-guided multimodal alignment, enriching its EO embeddings with functional meaning and advancing toward general-purpose urban representations that couple physical form with human environment.

### 3. Methodology

The proposed framework adapts the AE model for urban applications through POI-guided multimodal alignment. Given a set of POIs with textual descriptions and spatial coordinates, and AE embedding maps produced from multi-source EO data (including multispectral, topographic, and auxiliary geospatial layers), the framework learns an embedding space that unifies visual and textual urban semantics. Specifically, AE provides spatially complete yet human-functionally limited 64-dimensional features at 10 m resolution, while POIs offer discrete but functionally rich textual cues. By aligning these two modalities, we inject human-centered semantics into the AE feature space, enabling general-purpose and semantically consistent urban representations.

As shown in Figure 1, the AETHER framework consists of three main components: (1) a POI text branch, which encodes POI descriptions into semantic embeddings via a pretrained language model and a lightweight projector; (2) an AE branch, which aggregates local AE embeddings around POI locations using multi-scale pooling and projects them into the same latent space; and (3) a contrastive alignment module, which jointly optimizes cross-modal (POI-AE) and intra-modal (multi-scale AE) consistency. During inference, only the AE projector is retained to produce semantically enriched spatial embeddings across the full city, which can be flexibly aggregated for downstream tasks.

#### 3.1. POI Encoder

Points of Interest (POIs) are widely used as proxies for human activities and urban functions. Recent studies, particularly the CaLLiPer series (Wang et al., 2025; Liu et al., 2025), have demonstrated that the rich semantic content

encoded in POI names and categories plays a crucial role in constructing meaningful city representations. Following this line of work, we employ a large language model (LLM) to extract semantic embeddings from POI text, thereby integrating fine-grained functional meanings into the multimodal representation space shared with AE features. The pretrained LLM provides contextualized semantics beyond categorical labels, capturing subtle variations in urban functions.

Formally, each POI record  $p_i$  is associated with a semantic description  $s_i$  that combines both its categorical type and its specific name. To capture fine-grained semantics, we construct an enriched description by concatenating the name  $n_i$ , first-level category  $t_{1i}$ , and second-level subcategory  $t_{2i}$  through a simple template:

$$s_i = \text{"A place of } [t_{2i}], \text{ a type of } [t_{1i}], \text{ named } [n_i].\text{"} \quad (1)$$

For example, a POI may be represented as “A place of *coffee shop*, a type of *food and drink*, named *Starbucks*.“ This formulation allows the model to capture both general functional categories and nuanced semantic distinctions between individual entities.

The pretrained language model  $E(\cdot)$  encodes each description into a contextualized embedding:

$$\mathbf{t}_i = E(s_i) \in \mathbb{R}^{d_t}, \quad (2)$$

where  $d_t$  denotes the encoder’s output dimension. To align with the shared multimodal space, we apply a single linear projector and  $\ell_2$  normalization:

$$\mathbf{z}_i^{\text{poi}} = \text{norm}(W_{\text{poi}} \mathbf{t}_i), \quad W_{\text{poi}} \in \mathbb{R}^{d \times d_t}. \quad (3)$$

This enriched text representation enables the model to encode both functional and entity-level semantics, improving its ability to differentiate between places with similar categories but distinct social or economic connotations.

### 3.2. AlphaEarth Encoder

AE (Brown et al., 2025) provides high-quality geospatial embeddings that integrate multi-source EO data through a unified space-time precision encoder. Each 10 m pixel on Earth’s surface is represented by a 64-dimensional embedding that summarizes local spectral, temporal, and environmental contexts within a defined temporal window. These embeddings are released as annualized “embedding field” layers on Google Earth Engine, forming a globally consistent and information-rich base for downstream mapping applications.

For each POI location  $p_i$ , we retrieve AE features from the embedding field at or around its coordinates. To incorporate local spatial context, we extract features within one or more spatial buffers centered at  $p_i$ . Specifically, we define a *base view* with radius  $r_b$  and an *augmented view* with a larger radius  $r_a > r_b$ . Average pooling is applied within each buffer to obtain two spatially aggregated feature vectors, i.e.,  $\mathbf{a}_i^{(b)}, \mathbf{a}_i^{(a)} \in \mathbb{R}^{64}$ . These features capture both fine-grained local textures and broader urban environmental patterns encoded in AE.

Each feature vector is then passed through a lightweight projection head  $f_\theta(\cdot)$ , implemented as a two-layer MLP with residual and gating connections followed by a post-MLP projection, and  $\ell_2$  normalization:

$$\mathbf{z}_i^{(b)} = \frac{f_\theta(\mathbf{a}_i^{(b)})}{\|f_\theta(\mathbf{a}_i^{(b)})\|_2}, \quad \mathbf{z}_i^{(a)} = \frac{f_\theta(\mathbf{a}_i^{(a)})}{\|f_\theta(\mathbf{a}_i^{(a)})\|_2}. \quad (4)$$

The outputs  $\mathbf{z}_i^{(b)}$  and  $\mathbf{z}_i^{(a)}$  correspond to normalized embeddings from the base and augmented spatial views, respectively, both lying on the unit hypersphere  $\mathbb{S}^{d-1}$ . This projection step adapts the 64-dimensional AE features into the shared latent space ( $d$ -dimensional) used for multimodal alignment with POI semantics.

By leveraging AE’s continuous and globally standardized embeddings, our model inherits rich spectral priors while remaining computationally efficient. This enables seamless adaptation from natural to urban domains, providing a comprehensive, semantically extensible representation for urban understanding.

### 3.3. Multimodal Contrastive Alignment

To inject functional semantics into AE embeddings, we align the AE and POI representations in a shared latent space through contrastive learning. For a batch of  $N$  POIs, we have triplets  $(\mathbf{z}_i^{(b)}, \mathbf{z}_i^{(a)}, \mathbf{z}_i^{\text{poi}})$ , where  $\mathbf{z}_i^{(b)}$  and  $\mathbf{z}_i^{(a)}$  denote the base and augmented AE embeddings, and  $\mathbf{z}_i^{\text{poi}}$  is the POI embedding. The alignment objective consists of two symmetric contrastive losses: an intra-modal AE context term and a cross-modal AE–POI alignment term.

(1) *Intra-modal AE consistency*. This term enforces representation stability across different spatial scales of the same location, encouraging the AE encoder to produce consistent embeddings for nearby contexts:

$$\mathcal{L}_{\text{AE}} = -\frac{1}{2N} \sum_{i=1}^N \left[ \log \frac{\exp(\mathbf{z}_i^{(b)\top} \mathbf{z}_i^{(a)}/\tau_{\text{ae}})}{\sum_{j=1}^N \exp(\mathbf{z}_i^{(b)\top} \mathbf{z}_j^{(a)}/\tau_{\text{ae}})} + \log \frac{\exp(\mathbf{z}_i^{(a)\top} \mathbf{z}_i^{(b)}/\tau_{\text{ae}})}{\sum_{j=1}^N \exp(\mathbf{z}_i^{(a)\top} \mathbf{z}_j^{(b)}/\tau_{\text{ae}})} \right], \quad (5)$$

where  $\tau_{\text{ae}}$  is a fixed temperature controlling the sharpness of the similarity distribution.

(2) *Cross-modal AE-POI alignment*. This term injects semantic meaning into AE embeddings by aligning them with POI representations in the shared latent space:

$$\mathcal{L}_{\text{AP}} = -\frac{1}{2N} \sum_{i=1}^N \left[ \log \frac{\exp(\mathbf{z}_i^{(b)\top} \mathbf{z}_i^{\text{poi}}/\tau_{\text{poi}})}{\sum_{j=1}^N \exp(\mathbf{z}_i^{(b)\top} \mathbf{z}_j^{\text{poi}}/\tau_{\text{poi}})} + \log \frac{\exp(\mathbf{z}_i^{\text{poi}\top} \mathbf{z}_i^{(b)}/\tau_{\text{poi}})}{\sum_{j=1}^N \exp(\mathbf{z}_i^{\text{poi}\top} \mathbf{z}_j^{(b)}/\tau_{\text{poi}})} \right], \quad (6)$$

where  $\tau_{\text{poi}}$  denotes the temperature for cross-modal alignment.

(3) *Overall objective*. The final training loss combines the two objectives with a balancing coefficient  $\lambda \in [0, 1)$ :

$$\mathcal{L} = \lambda \mathcal{L}_{\text{AE}} + (1 - \lambda) \mathcal{L}_{\text{AP}}. \quad (7)$$

This joint optimization ensures that AE embeddings remain spatially coherent while being semantically enriched by POI guidance. The model is optimized using AdamW with fixed temperatures and the best checkpoint is selected based on the lowest cross-modal alignment loss.

### 3.4. Downstream Tasks: LUC and SDM

After training, the aligned AE encoder  $f_\theta$  is applied across AE pixels to produce comprehensive, semantically informed embeddings. To construct region-level representations, we aggregate base-view embeddings within each spatial unit (e.g., administrative area, buffer, or grid cell) by mean pooling:

$$\mathbf{r}_k = \frac{1}{N_k} \sum_{u \in \text{region } k} \mathbf{z}_u^{(b)} \in \mathbb{R}^d. \quad (8)$$

We then attach a lightweight task head  $h_\psi(\cdot)$  on top of the region embedding  $\mathbf{r}_k$ . Unless otherwise stated,  $h_\psi$  is implemented as a two-layer MLP with one hidden layer:

$$\mathbf{h}_k = \sigma(W_1 \mathbf{r}_k + \mathbf{b}_1), \quad \boldsymbol{\ell}_k = W_2 \mathbf{h}_k + \mathbf{b}_2, \quad (9)$$

where  $\sigma(\cdot)$  is the ReLU activation, and  $\{W_1, W_2, \mathbf{b}_1, \mathbf{b}_2\}$  are task-specific parameters. A purely linear head is obtained as a special case by removing the hidden layer and directly applying  $W_2$  to  $\mathbf{r}_k$ . For classification tasks, a log-softmax is applied to the output logits, whereas for regression tasks, the raw outputs are used directly.

#### 3.4.1. Land-Use Classification (LUC)

The LUC task aims to predict the dominant land-use category of a given spatial unit based on its embeddings. Each region (or sample point) is associated with one of  $C$  land-use categories derived from the NLUD dataset (Section 4.1). For each region  $k$ , the aggregated representation  $\mathbf{r}_k$  is passed through the task head  $h_\psi(\cdot)$  to obtain logits  $\boldsymbol{\ell}_k$ , which are converted to class probabilities via the softmax function:

$$\mathbf{p}_k = \text{softmax}(\boldsymbol{\ell}_k) \in \Delta^{C-1}. \quad (10)$$

Given the ground-truth label  $y_k \in \{1, \dots, C\}$ , the model is trained with the cross-entropy objective:

$$\mathcal{L}_{\text{LUC}} = -\frac{1}{|\mathcal{D}|} \sum_{k \in \mathcal{D}} \log \mathbf{p}_k[y_k]. \quad (11)$$

The training and test splits follow the same random partition protocol as all baselines to ensure comparability. Performance is evaluated on the held-out test set using macro-averaged Precision, Recall, and F1 score across the ten land-use categories.

### 3.4.2. Socioeconomic Distribution Mapping (SDM)

For distributional targets (e.g., binned population densities) with target histogram  $\mathbf{q}_k \in \Delta^{B-1}$ , the head produces a categorical distribution  $\mathbf{p}_k = \text{softmax}(\ell_k)$ . We optimize the likelihood-based cross-entropy

$$\mathcal{L}_{\text{SDM}} = -\frac{1}{|\mathcal{D}|} \sum_{k \in \mathcal{D}} \mathbf{q}_k^\top \log \mathbf{p}_k, \quad (12)$$

which is equivalent to minimizing  $\text{KL}(\mathbf{q}_k \parallel \mathbf{p}_k)$  up to a constant. Evaluation follows prior work and reports  $L_1$ , Chebychev distance, and KL divergence between predicted and reference distributions. For scalar regression variants, we use the same MLP form in Eq. (9) without softmax and optimize a regression loss (e.g., MSE) on standardized targets.

*Training protocol.* Task heads are trained on learned region embeddings  $\{\mathbf{r}_i\}_{i=1}^n$  using Adam with early stopping on validation loss. All downstream training and evaluation use the same random split protocol as baselines to ensure comparability.

## 4. Experimental Setup

### 4.1. Study Area and Datasets

We conduct experiments in London (UK), a metropolitan region characterized by diverse land use patterns and socioeconomic structures. We use the AE embeddings, providing 64-dimensional features at 10 m spatial resolution (Section 3.2). All geospatial datasets are reprojected to a unified coordinate reference system before feature extraction. POIs are stored as GeoDataFrames and include a description field combining names and hierarchical categories for text encoding.

*Data sources.*

- AlphaEarth embeddings<sup>1</sup>. 64D embeddings at 10 m spatial resolution from the AE model (Brown et al., 2025), representing multi-source EO features. These embeddings are used as the base EO representations for multimodal alignment and downstream inference.
- Ordnance Survey POI (OS POI)<sup>2</sup>. Each POI record contains geographic coordinates, a name, and hierarchical category labels. These POIs provide semantically rich textual supervision for multimodal contrastive pretraining and human-centered representation learning.
- Verisk National Land Use Database (NLUD)<sup>3</sup>. Provides polygonal land-use delineations across the UK. Each polygon is assigned to one of ten major land-use categories (e.g., residential, commercial, industrial). In this study, the NLUD data serve as the ground truth for the LUC task.
- Office for National Statistics (ONS) 2021 Census<sup>4</sup>. Contains detailed socioeconomic information at the Lower-layer Super Output Area (LSOA) level. We use the National Statistics Socioeconomic Classification (NS-SeC) with nine occupational bins (ns-sec\_1-ns-sec\_9), normalized to sum to one. These data provide the ground truth for the SDM task.

All geospatial layers are reprojected to the British National Grid (EPSG:27700). POI records are cleaned and linked with hierarchical taxonomies, constructing a unified description field combining name, primary, and secondary categories for text encoding. For SDM, NS-SeC occupational counts are row-normalized into probability vectors  $\mathbf{q}_k \in \Delta^8$ . All datasets are clipped to the London administrative boundary to ensure spatial consistency in sampling and alignment.

<sup>1</sup><https://earthengine.google.com/>

<sup>2</sup><https://digimap.edina.ac.uk/>

<sup>3</sup><https://digimap.edina.ac.uk/roam/map/verisk>

<sup>4</sup><https://www.ons.gov.uk/>

#### 4.2. Pretraining Setup

The multimodal alignment between AE and POI embeddings follows the formulation in Section 3.3. Each POI is associated with two spatial views: a *base buffer* of 50 m ( $r_b$ ) and an *augmented buffer* of 100 m ( $r_a$ ). The total loss is defined as  $\mathcal{L} = \lambda \mathcal{L}_{AE} + (1 - \lambda) \mathcal{L}_{AP}$ , where  $\lambda = 0.2$ ,  $\tau_{ae} = \tau_{poi} = 0.07$ . We employ the AdamW optimizer with a batch size of 512. The projection head consists of a single hidden layer (256 units) and an output dimension of 128. Training is performed on a single NVIDIA TITAN (24 GB) GPU for 100 epochs, and the checkpoint with the lowest cross-modal loss on the training set is selected (“best-on-train”).

#### 4.3. Analysis Units and Spatial Aggregation

All experiments are conducted in London. For LUC, we randomly sample points from ten major land-use categories defined by the NLUD. Each sample point is represented by the mean-pooled AE embeddings within a 50 m spatial buffer, providing localized morphological context. For SDM, analysis is performed at the LSOA level, where each region is represented by the AE embeddings averaged within a 300 m buffer centered on the population-weighted centroid.

#### 4.4. Baselines

We compare AETHER with a range of representative baselines covering semantic, spatial, POI-based multimodal, and EO-driven urban representation models:

- Classical semantic baselines: TF-IDF (Sparck Jones, 1972) and LDA (Blei et al., 2003), which construct region-level textual features based on the frequency and co-occurrence of POI categories, serving as simple yet interpretable semantic baselines.
- POI-based models: Place2Vec (Yan et al., 2017), Doc2Vec (Niu and Silva, 2021), SPPE (Huang et al., 2022), and HGI (Huang et al., 2023), which learn urban representations from POI distributions, spatial co-occurrences, or graph-structured relations.
- Coordinate-based spatial encoders: Space2Vec (Mai et al., 2020) encodes locations through positional embeddings and neural encoders, learning continuous spatial representations directly from geographic coordinates.
- Multimodal POI–location alignment: CaLLiPer (Wang et al., 2025; Liu et al., 2025) aligns POI text embeddings with spatial coordinates via contrastive learning, providing a strong baseline for urban functional and socioeconomic mapping tasks.
- Earth-observation (EO) foundation models: SatCLIP (Klemmer et al., 2023) and AlphaEarth (Brown et al., 2025) learn embeddings from multi-source satellite imagery. AlphaEarth, in particular, produces 64-dimensional embeddings at 10 m resolution with multi-source EO data, effectively capturing land-surface morphology and environmental context.

#### 4.5. Evaluation Metrics

We evaluate AETHER using task-specific metrics tailored to the two downstream settings. For all metrics,  $\uparrow$  indicates that higher values denote better performance, while  $\downarrow$  indicates the opposite.

*Land-Use Classification.* LUC is a multi-class classification task where each unit is assigned one of ten land-use categories. We use standard classification metrics computed on the test set:

- Precision: Precision =  $\frac{TP}{TP+FP}$ , measuring the proportion of correctly predicted positives among all predicted positives.
- Recall: Recall =  $\frac{TP}{TP+FN}$ , measuring the proportion of true positives among all ground-truth positives.
- F1 score: F1 =  $\frac{2 \times \text{Precision} \times \text{Recall}}{\text{Precision} + \text{Recall}}$ , balancing precision and recall to reflect overall classification accuracy.

*Socioeconomic Distribution Mapping.* SDM is formulated as a distribution regression task where the target is a normalized occupation distribution  $\mathbf{q}_k \in \Delta^8$  for each region. We evaluate the similarity between predicted and ground-truth distributions using:

- $L_1$  distance:  $L_1 = \frac{1}{N} \sum_{i=1}^N |p_i - q_i|$ , measuring the mean absolute difference between predicted and observed distributions.
- Chebyshev distance:  $L_\infty = \max_i |p_i - q_i|$ , capturing the maximum deviation across distribution bins.
- Kullback–Leibler divergence (KL):  $\text{KL}(\mathbf{q} \parallel \mathbf{p}) = \sum_i q_i \log \frac{q_i}{p_i}$ , quantifying information loss between predicted and true distributions.

#### 4.6. Sensitivity Study

We evaluate the robustness of the proposed framework with respect to three key factors, varying one factor at a time while keeping the others fixed at the canonical configuration ( $\lambda=0.2$ ,  $r_b=50$  m,  $r_a=100$  m, full training set). All experiments follow the same protocol and evaluation metrics described in Section 4.5.

**Loss balance ( $\lambda$ ).** We sweep the contrastive weighting coefficient  $\lambda \in \{0.0, 0.1, \dots, 0.9\}$  in  $\mathcal{L} = \lambda \mathcal{L}_{\text{AE}} + (1-\lambda) \mathcal{L}_{\text{AP}}$  to examine how the trade-off between intra-modal AE consistency and POI-guided cross-modal alignment affects performance.

**Spatial scale.** To assess the effect of spatial context, we vary the buffer radii used for AE feature aggregation:  $r_b \in \{25, 50\}$  m for the base buffer and  $r_a \in \{50, 75, 100, 125\}$  m for the augmented buffer ( $r_a > r_b$ ). When one radius is varied, the other is fixed to its default.

**Training supervision.** We test data efficiency by subsampling the training set to different proportions of available POI–AE pairs (e.g., 10%, 20%, …, 100%), sampled uniformly with a fixed random seed.

These one-factor experiments collectively examine the sensitivity of AETHER to objective weighting ( $\lambda$ ), spatial context ( $r_b, r_a$ ), and supervision scale (training POIs). Quantitative results are reported in Section 5.

## 5. Results

### 5.1. Performance on Downstream Tasks

Table 1 summarizes the results of AETHER and all baselines on the LUC and SDM tasks in London. After integrating POI semantics through multimodal alignment, AETHER achieves the best overall results across both tasks. In LUC, it raises F1 from 56.6 to 60.7, yielding a 7.2% relative F1 improvement over AE. In SDM, AETHER lowers KL divergence from 43.2 to 33.0 (a 23.6% reduction) and  $L_1$  from 21.7 to 18.8 (a 13.4% reduction). These consistent gains indicate that POI-guided alignment successfully injects human-functional semantics into the EO feature space, allowing the model to reason not only about what the city looks like but also what it is used for.

The ablated variant without the augmented AE branch (AETHER w/o aug) performs relatively worse on both tasks, highlighting the additional contribution of the multi-scale projection design. Compared with the strongest external baseline (SOTA), the full AETHER achieves a relative improvement of 61.4% in LUC and a reduction of 11.8% in KL for SDM, whereas its single-scale counterpart attains 60.9% and 8.8%, respectively. This indicates that incorporating the dual spatial buffers provides an additional 0.5% F1 gain and 3.0% KL reduction, demonstrating that the scale-consistency term  $\mathcal{L}_{\text{AE}}$  effectively enriches contextual perception around each POI and improves cross-modal alignment robustness.

The performance improvement of AE and AETHER varies in tasks as shown in Figure 2. For LUC (higher is better), AE already outperforms the best non-EO baseline by a large margin (+50.5% relative F1 over CaLLiPer+), reflecting that morphological and spectral cues captured by EO embeddings are highly informative for land-use differentiation. AETHER brings a further gain over AE in this setting (+61.4% relative vs. CaLLiPer+), indicating that additional semantics provide moderate extra benefit when physical texture already dominates the signal.

In contrast, for SDM (lower KL is better), AE lags behind the best non-EO baseline (−15.5% relative change vs. CaLLiPer+), highlighting a lack of human-centered contextual information in purely EO-driven features. By aligning with POI semantics, AETHER achieves an 11.8% relative reduction in KL over CaLLiPer+, substantially improving

Table 1: Comparison on LUC and SDM tasks in London. All metrics are reported as mean  $\pm$  std over five random seeds. For LUC, higher values indicate better performance; for SDM, lower values are better. To ensure comparable numeric ranges, all LUC metrics (F1, precision, recall) are scaled by  $10^2$ , while for SDM,  $L_1$  distances are scaled by  $10^2$  and both KL divergence and Chebyshev distances are scaled by  $10^3$ . Best, second-best, and third-best results are shown in **bold**, underlined, and *italic*, respectively.

Model	LUC ( $\uparrow$ )			SDM ( $\downarrow$ )		
	F1	Precision	Recall	KL	$L_1$	Chebyshev
TF-IDF	$31.7 \pm 0.6$	$31.8 \pm 0.6$	$33.3 \pm 0.5$	$52.0 \pm 0.4$	$24.4 \pm 0.2$	$72.8 \pm 0.5$
LDA	$29.2 \pm 0.9$	$31.5 \pm 1.1$	$30.4 \pm 0.7$	$58.0 \pm 7.2$	$25.9 \pm 0.1$	$77.7 \pm 11.2$
Space2Vec	$27.8 \pm 0.3$	$29.6 \pm 0.6$	$28.9 \pm 0.5$	$50.0 \pm 0.8$	$23.6 \pm 0.2$	$71.2 \pm 0.9$
Place2Vec	$32.4 \pm 1.2$	$35.1 \pm 1.2$	$32.7 \pm 1.0$	$46.1 \pm 0.2$	$22.8 \pm 0.1$	$68.1 \pm 0.1$
Doc2Vec	$32.7 \pm 0.6$	$34.9 \pm 0.9$	$33.8 \pm 0.5$	$47.5 \pm 0.8$	$23.1 \pm 0.2$	$68.9 \pm 0.6$
SPPE	$32.2 \pm 0.5$	$34.5 \pm 0.9$	$32.9 \pm 0.7$	$49.1 \pm 0.7$	$23.6 \pm 0.2$	$70.4 \pm 0.6$
HGI	$31.6 \pm 0.7$	$33.6 \pm 0.5$	$32.0 \pm 0.9$	$46.0 \pm 0.2$	$22.7 \pm 0.1$	$68.0 \pm 0.2$
CaLLiPer+	$37.6 \pm 0.3$	$41.3 \pm 0.7$	$37.8 \pm 0.4$	$37.4 \pm 0.1$	$19.4 \pm 0.0$	$58.3 \pm 0.4$
SatCLIP	$12.2 \pm 1.6$	$12.2 \pm 1.5$	$16.8 \pm 2.0$	$70.7 \pm 0.1$	$28.9 \pm 0.1$	$88.4 \pm 0.3$
AlphaEarth	$56.6 \pm 0.5$	$58.3 \pm 0.6$	$57.3 \pm 0.5$	$43.2 \pm 0.6$	$21.7 \pm 0.1$	$65.9 \pm 0.2$
AETHER (ours)	<b><math>60.7 \pm 0.4</math></b>	<b><math>61.4 \pm 0.3</math></b>	<b><math>60.7 \pm 0.3</math></b>	<b><math>33.0 \pm 0.3</math></b>	<b><math>18.8 \pm 0.1</math></b>	<b><math>56.2 \pm 0.1</math></b>
AETHER (w/o aug)	<u><math>60.5 \pm 0.2</math></u>	<u><math>60.5 \pm 0.2</math></u>	<u><math>60.1 \pm 0.2</math></u>	<u><math>34.1 \pm 0.4</math></u>	<u><math>19.1 \pm 0.1</math></u>	<u><math>57.2 \pm 0.3</math></u>

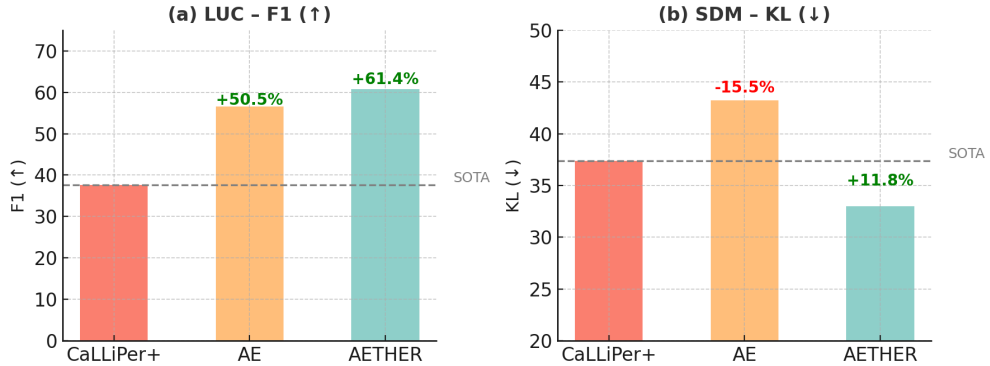


Figure 2: Comparison of AETHER, AlphaEarth (AE), and the strongest external baseline (SOTA). (a) Land-Use Classification (LUC, F1 $\uparrow$ ). (b) Socioeconomic Distribution Mapping (SDM, KL $\downarrow$ ). Dashed gray lines denote SOTA performance. Numbers above bars indicate relative changes compared with SOTA.

socioeconomic distribution mapping. Together, these results support our claim: EO embeddings suffice for physically grounded tasks like LUC, but injecting human-centered semantics is crucial for socially grounded tasks like SDM.

In summary, while AE alone provides strong visual representations, aligning it with POI semantics substantially enhances its functional knowledge. The resulting multimodal embeddings generalize better across land-use types and capture socioeconomic patterns more faithfully, demonstrating the effectiveness of coupling physical morphology with human-centered semantics in urban representation learning.

## 5.2. Sensitivity and Robustness

We conduct a systematic sensitivity and robustness analysis of the proposed AETHER framework with respect to its key hyperparameters and training supervision. Specifically, we vary (i) the loss balance coefficient  $\lambda$ , (ii) the base and augmented buffer radii ( $r_b, r_a$ ), and (iii) the proportion of POI–AE pairs used for training.

### 5.2.1. Effect of loss weight

As shown in Figure 3, overall performance on LUC–F1 ( $\uparrow$ ) and SDM–KL ( $\downarrow$ ) is highest at a relatively small loss weight ( $\lambda=0.2$ ). When  $\lambda$  increases, performance on both tasks gradually declines, indicating that large-scale AE

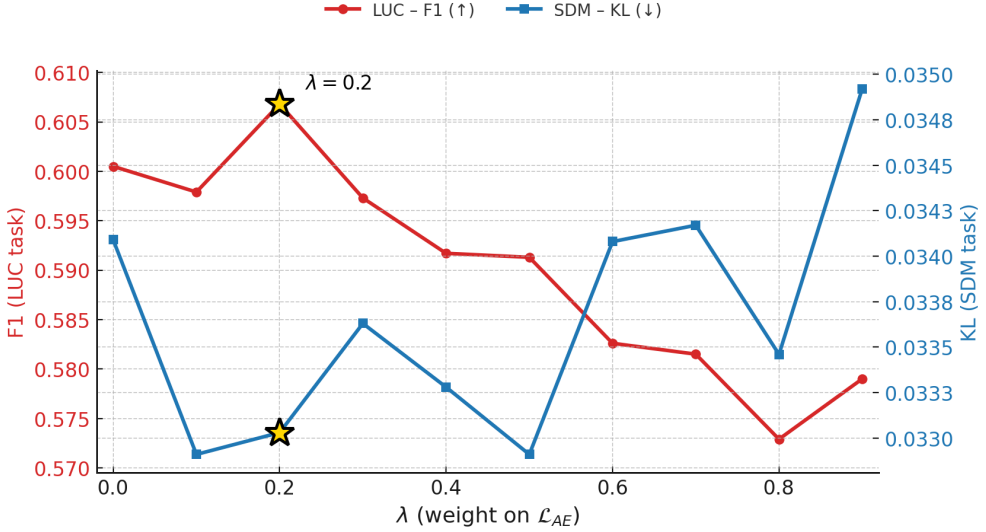


Figure 3: Sensitivity to the loss balance coefficient  $\lambda$ .

Table 2: Effect of base and augmented buffer radii ( $r_b, r_a$ ) on LUC and SDM tasks. All metrics are reported with four decimal places. F1 ( $\uparrow$ ) and KL ( $\downarrow$ ) correspond to performance on LUC and SDM, respectively.

$r_b$ (m)	$r_a$ (m)	LUC-F1 ( $\uparrow$ )	SDM-KL ( $\downarrow$ )
25	50	0.5977	0.0352
25	75	0.5872	0.0336
25	100	0.5867	0.0339
50	75	0.6035	0.0333
<b>50</b>	<b>100</b>	<b>0.6068</b>	<b>0.0330</b>
50	125	0.5841	0.0333

self-alignment serves primarily as an auxiliary signal. Excessive emphasis on intra-modal AE consistency weakens POI-guided semantic grounding, leading to over-regularization and semantic drift. Conversely, a smaller  $\lambda$  allows the model to focus on the base AE representation while preserving sufficient cross-modal supervision from POIs. This moderate balance yields the most effective semantic alignment, and thus  $\lambda=0.2$  is adopted for all subsequent experiments.

#### 5.2.2. Effect of spatial scale

Table 2 summarizes the results obtained with different combinations of base and augmented buffer radii ( $r_b, r_a$ ). The model exhibits stable performance across all settings, demonstrating the importance of spatial scale choices. The combination  $r_b=50$  m and  $r_a=100$  m yields the best overall results for both LUC and SDM. This setting aligns with the spatial footprint of most urban POIs, where a 50 m base buffer effectively captures the core semantics of a site, and a 100 m augmented buffer incorporates its immediate contextual environment. Such a configuration provides a balanced representation between fine-grained local detail and broader spatial context, ensuring consistent generalization across urban morphologies.

#### 5.2.3. Effect of data volume

Figure 4 analyzes how varying the proportion of POI–AE training pairs affects model performance. For the LUC task, the F1 score remains largely stable across a wide range of training ratios, reflecting that the AE backbone already encodes highly informative and transferable spatial representations. Because LUC is strongly driven by physical land-cover cues, insufficient alignment may introduce mild spatial noise that interferes with existing AE structure, while

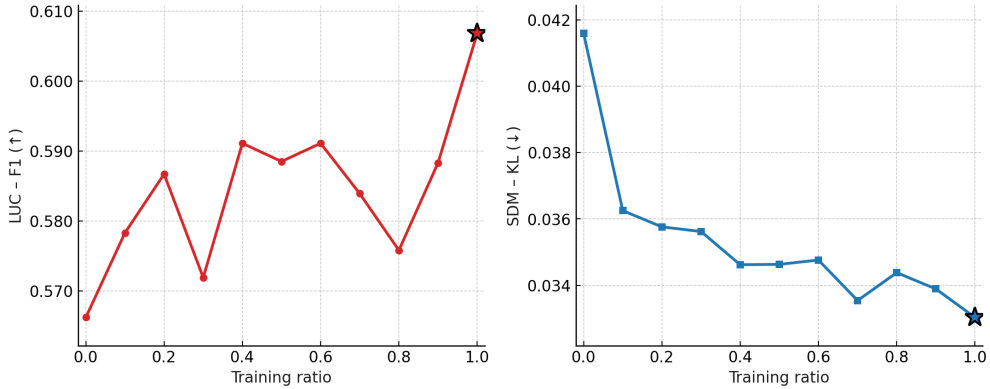


Figure 4: Model performance under varying training data volumes.

sufficient POIs improve the performance. In contrast, the SDM task exhibits a clear and consistent improvement as the training ratio increases: the KL divergence steadily decreases, indicating that stronger POI–AE alignment injects richer semantic priors for socioeconomic distribution estimation. Notably, even with as little as 10% of the available POI–AE pairs, AETHER aligns the cross-modal space effectively. This demonstrates that the learned alignment mechanism generalizes well under sparse supervision, ensuring both robustness and data efficiency.

### 5.3. Efficiency and Scalability

Benefiting from its lightweight architecture and streamlined alignment design, the AETHER framework demonstrates excellent computational efficiency in both training and inference. Using a single NVIDIA TITAN (24 GB) GPU, alignment training with approximately 340k POI samples over 100 epochs takes only about 502 seconds in total—roughly 5 seconds per epoch. During inference, feature generation is highly efficient, as representations are produced directly from precomputed AE embeddings through a lightweight alignment module with minimal computational overhead. These results highlight the strong practical feasibility of AETHER, showing that it maintains high representational quality while remaining scalable to city-level applications.

## 6. Discussion

*What AlphaEarth captures and what it does not.* The AE foundation model provides a strong baseline for urban analysis. Its multisource embeddings capture fine-grained morphological and land-cover patterns, which explain its strong performance on physically grounded tasks such as LUC. AE effectively encodes surface texture, vegetation, built form, and other optical–structural cues, enabling high spatial differentiation across urban areas. However, its representations remain largely visual and physical in nature. Socioeconomic attributes such as occupation structure, income, or service accessibility are only weakly reflected in remote sensing features. As a result, AE shows limited effectiveness on tasks like SDM, where variations stem more from human activities than from spectral or morphological appearance. This reveals a fundamental gap: while AE provides excellent spatial continuity and environmental coverage, it lacks the human-centric semantics required for comprehensive urban understanding.

*Why AETHER works.* The AETHER framework addresses this limitation by coupling AE’s physical priors with the functional information embedded in POI text. This cross-modal alignment enriches AE embeddings with additional cues about human activity and service function, without sacrificing spatial coverage. AE provides morphologically informed features, while POIs contribute discrete yet semantically grounded supervision signals. A moderate alignment weight ( $\lambda=0.2$ ) proves most effective, suggesting that AE’s self-consistency should act as a regularizer rather than dominate learning. The dual-buffer design with a base radius of 50 m and an augmented radius of 100 m, capturing both the focal POI footprint and its immediate surroundings, effectively supplementing the local feature space with broader spatial context. This complementary structure allows AETHER to perceive not only the intrinsic characteristics of a site but also its environmental background, aligning well with typical urban spatial scales. Together, these

design choices enable AETHER to learn representations that bridge physical form and functional meaning, enhancing both LUC and SDM performance.

*Robustness and data efficiency.* Sensitivity experiments show that AETHER is robust across a wide range of hyper-parameters and supervision levels. LUC accuracy remains stable even with limited training data, confirming that AE already encodes strong land-use signals and that moderate POI supervision suffices to align semantic consistency. SDM performance, on the other hand, steadily improves with larger training ratios, reflecting the increasing benefit of POI–AE alignment for socially grounded tasks. Even when trained with as little as 10–30% of available POI–AE pairs, AETHER preserves most of full-data accuracy. The framework is also insensitive to reasonable variations in spatial buffer sizes, indicating strong generalizability and scalability across urban morphologies. These findings suggest that AETHER can adapt effectively under sparse supervision and maintain stable performance across different spatial configurations.

*Limitations and Future Directions.* While the proposed framework demonstrates strong empirical performance, several aspects warrant further investigation. First, the current experiments focus on the Greater London region and two representative downstream tasks—land-use classification and socioeconomic distribution mapping. Future work should extend the evaluation to other cities, spatial scales, and task domains to more comprehensively assess generalizability across diverse urban morphologies and policy contexts. Second, POI data are inherently uneven in density and subject to category bias; their naming conventions and taxonomies also evolve over time, which may lead to temporal inconsistencies with AE vintages and introduce alignment noise. Third, the present multimodal design focuses on coupling AE embeddings with POI semantics, whereas additional modalities such as road networks, mobility traces, and street-view imagery could further enrich the representation space by capturing complementary spatial and behavioral cues. Lastly, interpretability remains an open challenge: although the alignment enhances functional and predictive capacity, it provides only limited insight into the specific human-centric semantics learned. Integrating concept attribution, probing analyses, and counterfactual reasoning could offer deeper interpretive understanding of multimodal urban representations.

*Potential.* Beyond the two evaluated tasks, the proposed framework can be readily extended to a wide range of downstream urban applications. Potential directions include urban function and morphology classification, socioeconomic and demographic inference, environmental and infrastructure assessment, and broader spatial decision-support tasks in planning and governance. By integrating physical and human-centered signals, AETHER offers a unified foundation for multimodal urban analytics and cross-domain transfer. Importantly, AETHER is a framework rather than a fixed model. It does not depend on any specific backbone for either EO or text encoding—both the AE and language encoders can be replaced as foundation models evolve. This modular and extensible design ensures long-term adaptability: as stronger geospatial or linguistic models emerge, AETHER can seamlessly inherit their advances while preserving its lightweight alignment mechanism. In this sense, it provides a generalizable recipe for bridging physical morphology and human semantics across the next generation of geospatial foundation models.

## 7. Conclusions

This study introduced AETHER, a simple yet effective framework that adapts the AE to human-centered applications through POI-guided multimodal alignment. By coupling the complete and spatially uniform embeddings of AE with the human-centric information encoded in POI text, AETHER produces functionally meaningful representations of urban space. The framework preserves the efficiency of EO backbones by employing multi-scale projection modules and using contrastive alignment to inject urban functional information. Experiments in Greater London demonstrate consistent improvements over all baselines, while maintaining strong robustness and high computational efficiency. Achieving state-of-the-art performance across multiple downstream tasks, AETHER highlights a practical pathway for transforming geospatial foundation models into general-purpose urban representations. In doing so, it effectively bridges physical morphology with socioeconomic function, providing a scalable foundation for multimodal urban understanding.

## References

Bai, L., Huang, W., Zhang, X., Du, S., Cong, G., Wang, H., Liu, B., 2023. Geographic mapping with unsupervised multi-modal representation learning from vhr images and pois. *ISPRS Journal of Photogrammetry and Remote Sensing* 201, 193–208.

Batty, M., 2013. The new science of cities. MIT press.

Blei, D.M., Ng, A.Y., Jordan, M.I., 2003. Latent dirichlet allocation. *Journal of machine Learning research* 3, 993–1022.

Brown, C.F., Kazmierski, M.R., Pasquarella, V.J., Ruckridge, W.J., Samsikova, M., Zhang, C., Shelhamer, E., Lahera, E., Wiles, O., Ilyushchenko, S., et al., 2025. Alphaearth foundations: An embedding field model for accurate and efficient global mapping from sparse label data. *arXiv preprint arXiv:2507.22291* .

Goodchild, M.F., 2020. Platial, in: *International Encyclopedia of Geography*. Wiley, pp. 1–5. doi:[10.1002/9781118786352.wbieg2046](https://doi.org/10.1002/9781118786352.wbieg2046).

Huang, W., Cui, L., Chen, M., Zhang, D., Yao, Y., 2022. Estimating urban functional distributions with semantics preserved poi embedding. *International Journal of Geographical Information Science* 36, 1905–1930.

Huang, W., Zhang, D., Mai, G., Guo, X., Cui, L., 2023. Learning urban region representations with pois and hierarchical graph infomax. *ISPRS Journal of Photogrammetry and Remote Sensing* .

Klemmer, K., Rolf, E., Robinson, C., Mackey, L., Rußwurm, M., 2023. Satclip: Global, general-purpose location embeddings with satellite imagery. *arXiv preprint arXiv:2311.17179* .

Liu, J., Wang, X., Cheng, T., 2025. Enriching location representation with detailed semantic information, in: 13th International Conference on Geographic Information Science (GIScience 2025), pp. 3:1–3:15. doi:[10.4230/LIPIcs.GIScience.2025.3](https://doi.org/10.4230/LIPIcs.GIScience.2025.3).

Mac Aodha, O., Cole, E., Perona, P., 2019. Presence-only geographical priors for fine-grained image classification, in: *Proceedings of the IEEE/CVF International Conference on Computer Vision*, pp. 9596–9606.

Mai, G., Janowicz, K., Hu, Y., Gao, S., Yan, B., Zhu, R., Cai, L., Lao, N., 2022. A review of location encoding for geoai: methods and applications. *International Journal of Geographical Information Science* 36, 639–673. doi:[10.1080/13658816.2021.2004602](https://doi.org/10.1080/13658816.2021.2004602).

Mai, G., Janowicz, K., Yan, B., Zhu, R., Cai, L., Lao, N., 2020. Multi-scale representation learning for spatial feature distributions using grid cells, in: *International Conference on Learning Representations*. URL: <https://openreview.net/forum?id=rJ1jdh4KDH>.

Mai, G., Xuan, Y., Zuo, W., He, Y., Song, J., Ermon, S., Janowicz, K., Lao, N., 2023. Sphere2vec: A general-purpose location representation learning over a spherical surface for large-scale geospatial predictions. *ISPRS Journal of Photogrammetry and Remote Sensing* 202, 439–462.

Niu, H., Silva, E.A., 2021. Delineating urban functional use from points of interest data with neural network embedding: A case study in greater london. *Computers, Environment and Urban Systems* 88, 101651.

Qin, Q., Ai, T., Xu, S., Zhang, Y., Huang, W., Du, M., 2025. Learning dual context aware poi representations for geographic mapping. *International Journal of Applied Earth Observation and Geoinformation* .

Qin, Q., Xu, S., Du, M., Li, S., 2022. Identifying urban functional zones by capturing multi-spatial distribution patterns of points of interest. *International Journal of Digital Earth* .

Radford, A., Kim, J.W., Hallacy, C., Ramesh, A., Goh, G., Agarwal, S., Sastry, G., Askell, A., Mishkin, P., Clark, J., et al., 2021. Learning transferable visual models from natural language supervision, in: *International conference on machine learning*, PMLR. pp. 8748–8763.

Rußwurm, M., Klemmer, K., Rolf, E., Zbinden, R., Tuia, D., 2024. Geographic location encoding with spherical harmonics and sinusoidal representation networks, in: The Twelfth International Conference on Learning Representations.

Sparck Jones, K., 1972. A statistical interpretation of term specificity and its application in retrieval. *Journal of documentation* 28, 11–21.

Su, Y., Zhong, Y., Liu, Y., Zheng, Z., 2023. A graph-based framework to integrate semantic object/land-use relationships for urban land-use mapping with case studies of chinese cities. *International Journal of Geographical Information Science* .

Vivanco Cepeda, V., Nayak, G.K., Shah, M., 2024. Geoclip: Clip-inspired alignment between locations and images for effective worldwide geo-localization. *Advances in Neural Information Processing Systems* 36.

Wang, X., Cheng, T., Law, S., Zeng, Z., Yin, L., Liu, J., 2025. Multi-modal contrastive learning of urban space representations from poi data. *Computers, Environment and Urban Systems* 120, 102299. doi:[10.1016/J.COMPENVURBSYS.2025.102299](https://doi.org/10.1016/J.COMPENVURBSYS.2025.102299).

Wen, Y., Cai, J., Ma, Q., Li, L., Chen, X., Webster, C., Zhou, Y., 2025. Mobclip: Learning general-purpose geospatial representation at scale. *arXiv preprint arXiv:2506.01297* .

Xu, Y., Zhou, B., Jin, S., Xie, X., Chen, Z., Hu, S., He, N., 2022. A framework for urban land use classification by integrating the spatial context of points of interest and graph convolutional neural network method. *Computers, Environment and Urban Systems* .

Yan, B., Janowicz, K., Mai, G., Gao, S., 2017. From itdl to place2vec: Reasoning about place type similarity and relatedness by learning embeddings from augmented spatial contexts, in: Proceedings of the 25th ACM SIGSPATIAL international conference on advances in geographic information systems, pp. 1–10.

Yan, Y., Wen, H., Zhong, S., Chen, W., Chen, H., Wen, Q., Zimmermann, R., Liang, Y., 2024. Urbanclip: Learning text-enhanced urban region profiling with contrastive language-image pretraining from the web, in: Proceedings of the ACM on Web Conference 2024, pp. 4006–4017.